

# Direct Reconstruction of Kinetic Parameter Images from Dynamic PET Data

M. Kamasak<sup>a</sup>                      C. A. Bouman<sup>a</sup>                      E. D. Morris<sup>b</sup>                      K. Sauer<sup>c</sup>  
kamasak@purdue.edu      bouman@ecn.purdue.edu      emorris@iupui.edu      sauer@nd.edu

<sup>a</sup> Purdue University Electrical and Computer Engineering Department

<sup>b</sup> Indiana University, Purdue University-Indianapolis Radiology and Biomedical Engineering Departments

<sup>c</sup> Notre Dame University Electrical and Computer Engineering Department

## Abstract

*It is often necessary to estimate the parameters of a compartmental model from PET image data. These kinetic parameters are important because they quantify physiological processes. Existing methods for computing kinetic parametric images work by first reconstructing a sequence of PET images, and then estimating the kinetic parameters for each voxel location in the images. We propose a novel iterative tomographic reconstruction algorithm for directly computing a MAP estimate of the kinetic parameter image directly from dynamic PET sinogram data. This MAP reconstruction process estimates a vector of kinetic parameters at each voxel using explicit models of measurement noise, temporal tracer concentration, and spatial parameter variation. Experimental simulations using a two tissue compartment model show that our method can substantially reduce parameter estimation error.*

## 1 Introduction

Many clinical applications of positron emission imaging (PET), such as heart perfusion, brain activation, and glucose utilization, require the measurement of temporal information about the tracer concentration. Typically, it is assumed that the tracer concentration in a voxel is governed by ordinary differential equations (ODE's) resulting from a compartmental model. Such models consist of compartments that represent kinetically distinct sources of radioactivity. The parameters of interest are then the rates of tracer exchange between the model's compartments. By solving the associated ODE's, it is easily shown that these model parameters are nonlinearly related to the observed tracer emission rates.

Current methods for estimating these model parameters divide the PET data into  $K$  time frames and reconstruct each frame independently. However, dividing the data decreases the amount of available data

for each frame, so the reconstructions of these frames tend to have very low SNR. To alleviate this problem, a region of interest (ROI) is typically selected and the voxels in the ROI are averaged for each frame to produce a single time-sequence of emission rates. A curve is then fit to this average time response and the model parameters of the ROI are estimated.

More recently, there has been interest in estimating parameters at each voxel by using regularization or clustering methods to spatially smooth the parameter estimates. (See [1] for an overview of such approaches.) However, these approaches suffer from the low SNR of individual time frame reconstructions.

In this paper, we propose an alternative method for computing dense estimates of the compartmental model parameters by directly reconstructing the parametric image from the entire PET data set. This approach has a number of advantages: a) It can improve SNR by integrating together the information from all the PET data using an appropriate noise model. b) It can accurately account for the point spread function of the PET system's forward model. c) It can more directly model the spatial variations of the actual model parameters, rather than simply spatially regularizing the emission rates themselves.

We use a realistic simulated phantom as the basis of a quantitative comparison between our method and conventional techniques that first form reconstructions at each time frame. Results indicate the the parametric reconstruction algorithm can substantially improve the accuracy of parameter estimates.

## 2 Compartmental Model

The physiological processes can often be modeled using compartmental models [2]. These models consist of compartments that represent physical spaces or different states of the tracer. The parameters of the model are then the rate of tracer exchange between the compartments. In this paper, we use a 2-tissue

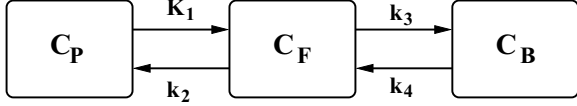


Figure 1: 2-tissue compartment model with 4 parameters

compartment model with 4 parameters. This model, shown in Fig. 1, is commonly used for FDG imaging and for high specific activity receptor-ligand imaging when there is no non-specific binding.

This model consists of 3 compartments: 1)  $C_P$ , the plasma compartment, represents the tracer concentration in the plasma 2)  $C_F$ , the free compartment, represents tracer concentration in the tissue that is not metabolized or bound 3)  $C_B$ , the bound compartment, represents tracer concentration in the tissue that is metabolized or bound. Typically, tracer in the plasma compartment can be measured by sampling blood during the scan. The quantities in this model obey the ODE's:

$$\frac{dC_F(t)}{dt} = K_1 C_P(t) - (k_2 + k_3) C_F(t) + k_4 C_B(t) \quad (1)$$

$$\frac{dC_B(t)}{dt} = k_3 C_F(t) - k_4 C_B(t) . \quad (2)$$

The PET signal is formed by the weighted sum of the tracer concentrations in the tissue and blood, appropriately attenuated by the decay rate of the isotope,  $\lambda$ ,

$$C_T(t) = C_F(t) + C_B(t) \quad (3)$$

$$f(K_1, k_2, k_3, k_4) = [(1 - V_B)C_T(t) + V_B C_P(t)] S_A e^{-\lambda t} \quad (4)$$

where  $S_A$  is the initial specific activity of the tracer.

Besides  $K_1$ ,  $k_2$ ,  $k_3$  and  $k_4$ , there are two more important parameters that can be derived from the model. These are the binding potential ( $BP$ ) and the volume of distribution ( $V_D$ ) given by

$$BP = \frac{k_3}{k_4} \quad (5)$$

$$V_D = \frac{K_1}{k_2} \left( 1 + \frac{k_3}{k_4} \right) . \quad (6)$$

These parametric images are also examined as a means of comparing methods.

### 3 Direct Reconstruction

Our proposed method reconstructs a single parametric image using the entire PET data set. The voxels of this image correspond to parameter vectors instead of emission intensities. More specifically, let  $\varphi_s$  be the 4-dimensional parameter vector at voxel  $s$ , and let  $\varphi$  be the parameter vectors at each voxel, which we

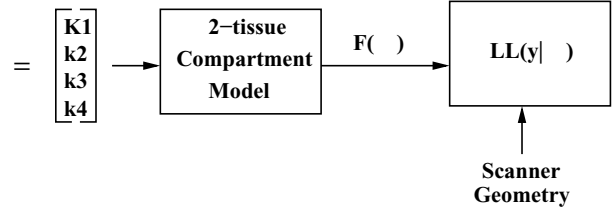


Figure 2: Direct reconstruction model

refer to as the parametric image. Then the emission rate at voxel  $s$  at each time frame is given by

$$f(\varphi_s) = [f(t_1, \varphi_s), f(t_2, \varphi_s), \dots, f(t_K, \varphi_s)]^t$$

where  $t_1, \dots, t_K$  are the  $K$  time frames, and we further define the function

$$F(\varphi) = [f(\varphi_1), f(\varphi_2), \dots, f(\varphi_N)]$$

to be the function which maps the parametric image to the emission rates for each voxel at each time. Using  $F(\varphi)$ , it is possible to compute  $LL(y|\varphi)$ , the log likelihood of the sinogram data  $y$  given  $\varphi$  based on a Poisson model of the sinogram counts.

Using the log likelihood, we form a cost functional

$$C(y|\varphi) = -LL(y|\varphi) + S(\varphi) \quad (7)$$

where  $S(\varphi)$  is a log prior or equivalently a stabilizing functional added to regularize the inversion. In the framework, the maximum a posteriori (MAP) reconstruction is given by

$$\hat{\varphi} = \arg \min_{\varphi} C(y|\varphi) \quad (8)$$

This reconstruction is computed efficiently by using pixel-wise iterated coordinate descent (PICD). This algorithm is similar to the ICD algorithm used in conventional PET image reconstruction methods[3], but it is adapted to account for the nonlinear parameters of the compartmental model. PICD sequentially updates the parameters of each voxel thereby monotonically decreasing the cost function given in Eq. (7). When  $F(\varphi)$  is a nonlinear function, the PICD algorithm reduces computation by decoupling the dependencies between the compartment model nonlinearities and the forward tomography model. We use the log prior from the Gaussian Markov random field model as the stabilizing function  $S(\varphi)$ .

In order to compute a PICD voxel update, we must compute

$$\varphi_s \leftarrow \arg \min_{\varphi_s} C(y|\varphi_s) . \quad (9)$$

To do this efficiently, we approximate the change in the cost functional as

$$\begin{aligned} \Delta C(y|\varphi_s) & \\ = -LL(y|\varphi_s) + LL(y|\tilde{\varphi}_s) + S(\varphi_s) & \quad (10) \\ \approx \sum_k (\theta_{1k}\Delta f_{sk} + \frac{1}{2}\theta_{2k}\Delta f_{sk}^2) + S(\varphi_s) & \end{aligned}$$

where  $\Delta f_{sk}$  is the change in the time response function of voxel  $s$  given as

$$\Delta f_{sk} = f(t_k, \varphi_s) - f(t_k, \tilde{\varphi}_s)$$

and  $\theta_{1k}$  and  $\theta_{2k}$  can be recursively updated using the same algorithm as in conventional ICD [3].

In order to further simplify the update computations, we re-parameterize the compartmental model from  $\varphi_s = [K_{1s}, k_{2s}, k_{3s}, k_{4s}]$  to  $\varphi_s = [a_s, b_s, c_s, d_s]$  to yield the time response

$$f(t_k, \varphi_s) = [(a_s e^{-c_s t} + b_s e^{-d_s t}) * C_P(t)]|_{t=t_k} S_A e^{-\lambda t_k}$$

where  $*$  indicates continuous time convolution, and  $\lambda$  is the tracer decay constant.

Since the parameters  $a_s$  and  $b_s$  are linear, there are closed form expressions for their PICD update in (9) when  $c_s$  and  $d_s$  are fixed. Substituting in these closed form expressions, we can write the PICD update as

$$\varphi_s \leftarrow \arg \min_{c_s, d_s} \tilde{C}(y|c_s, d_s). \quad (11)$$

In order to enforce uniqueness in the solution and stability of the model, we add the constraint that  $d_s \leq c_s$  and  $d_s \geq 0$ . The update of (11) can then be replaced with two coordinate-wise updates given by

$$\begin{aligned} c_n & \leftarrow \arg \min_{\{c_s: c_s \geq d_s\}} \tilde{C}(y|c_s, d_s) \\ d_n & \leftarrow \arg \min_{\{d_s: 0 \leq d_s \leq c_s\}} \tilde{C}(y|c_s, d_s). \end{aligned}$$

The reconstructions are initialized using a multi-resolution scheme. Coarsest resolution is initialized with a user selected constant. The reconstruction of each resolution is used to initialize the reconstructions of the next level of finer resolution. We used 3 levels of resolutions,  $32 \times 32$ ,  $64 \times 64$  and  $128 \times 128$ .

## 4 Simulations

A rat phantom is used for simulations. This phantom has 7 regions including the background. These regions are obtained by segmenting MRI scans of a rat through automated and manual techniques [4]. The regions and their corresponding parameters [5] are given in Table 1 and their time activity curves are

Region	$K_1$ $\frac{ml}{g \text{ min}}$	$k_2$ $\frac{1}{min}$	$k_3$ $\frac{1}{min}$	$k_4$ $\frac{1}{min}$
Background	0	0	0	0
CSF	0	0	0	0
Nonbrain	.1836	.8968	0	0
Whole brain	.0918	.4484	0	0
Striatum	.0918	.4484	1.2408	.1363
Cortex	.0918	.4484	.141	.1363
White matter	.02295	.4484	0	0

Table 1: Rat simulation

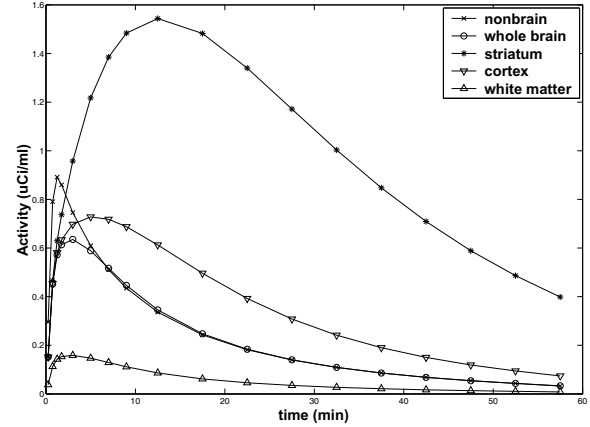


Figure 3: Time-activity curves for distinct regions in rat phantom.

shown in Fig. 3. Time frames of emission images are generated using these parameter images and the 2-tissue compartment model equations. The blood contribution to the PET activity is assumed to be zero and raclopride with  $^{11}C$  is assumed to be used as the tracer. The decay constant is  $\lambda = 0.034 \text{ min}^{-1}$ . Total scan time is 60 min., divided into 18 time frames as  $4 \times 0.5 \text{ min}$ ,  $4 \times 2 \text{ min}$  and  $10 \times 5 \text{ min}$ . The blood function,  $C_P(t)$ , is generated using equation (2) from reference [6].

These images are forward projected into sinograms for each frame using a Poisson model for the detected counts. Each sinogram consists of 180 angles and 200 radial bins per angle. A triangular point spread function with 4 mm base width is used in forward projections. The blood function,  $C_p(t)$  was scaled so that the total number of counts in all sinogram frames was approximately 10 million.

The proposed parametric reconstruction method is compared with pixel-wise methods for parametric estimation. The pixel-wise methods use reconstructed emission image frames to obtain the time response

function of each voxel. Estimation is done by weighted non-linear least-squares fitting of the model in Eq. (4) to the data at every voxel. This method is called pixel-wise weighted least squares method (PWLS). The PWLS with regularization (PWLSR) uses spatial regularization to smooth the estimates. For the pixel-wise methods, emission images are reconstructed using filtered backprojection (FBP).

The parameters are estimated only inside of a circular mask to reduce the estimation time. This mask is slightly bigger than the rat head and can be seen easily in the parametric image reconstructions.

In Fig. 4 the reconstructions of the re-organized parameters are shown. The PWLS method has created high variance estimations especially for nonlinear parameters,  $c$  and  $d$ . PWLSR can reduce this variation using the stabilizing function. The reconstructions of the parametric reconstructions are visually much better than the pixel-wise methods.

In Fig. 5 the reconstructions of the original parameters are shown. They are calculated using back transforms from  $a$ ,  $b$ ,  $c$ , and  $d$ . In this domain, the proposed parametric reconstruction method outperforms the pixel-wise techniques.

The normalized root mean squared errors (RMSE) for these parameters are given in Fig. 6. The RMSE of each parameter is normalized to the RMSE of the PWLS method. From this figure, it can be seen that the proposed method has uniformly lower RMSE in all parameters.

In Fig. 7 reconstructions of clinically important parameters are shown. These images are calculated using the equations given in Eq. (5) and Eq. (6). The improvement of the proposed methods on these parametric images can also be seen.

Finally, in Fig. 8 emission images reconstructed by FBP and created by using emission images are shown. There is a big improvement in the emission images calculated using the parametric images. Since each FBP frame is reconstructed using the corresponding sinogram frame, only a small portion of the entire dynamic PET data is used. However, each reconstruction calculated from the parametric images is obtained using the entire PET data set. Therefore the SNR in these images is substantially improved.

## 5 Conclusions

In this paper, we proposed a method for reconstruction of dense parametric images directly from the dynamic PET data. Using an anatomically and physiologically realistic small animal phantom, we demonstrated that our method can reduce the mean squared error in model parameter estimates.

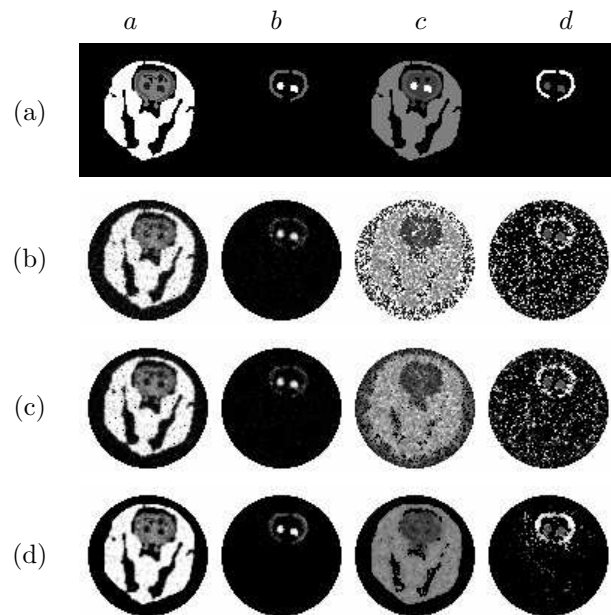


Figure 4: Parametric images of  $a$ ,  $b$ ,  $c$  and  $d$  estimated by the algorithms; (a) original (b) PWLS (c) PWLSR (d) parametric reconstruction (new method)

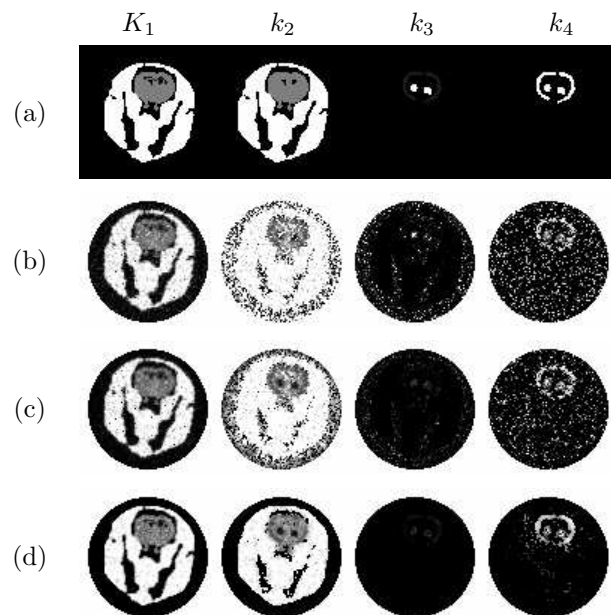


Figure 5: Parametric images of  $K_1$ ,  $k_2$ ,  $k_3$  and  $k_4$  estimated by the algorithms; (a) original (b) PWLS (c) PWLSR (d) parametric reconstruction (new method)

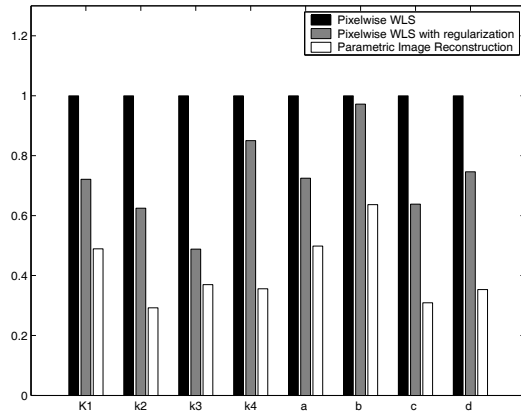


Figure 6: Normalized RMSE for the reconstructed parametric images

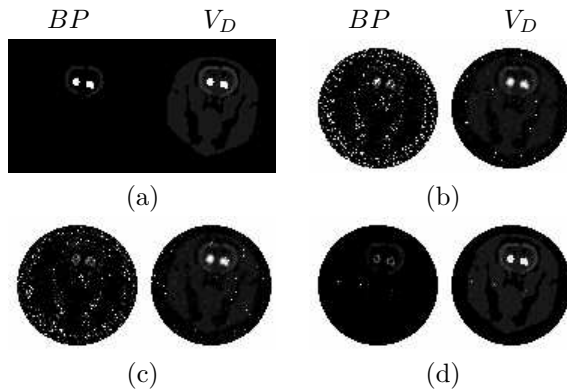


Figure 7: Parametric images of  $BP$  and  $V_D$  estimated by the algorithms; a) original (b) PWLS (c) PWLSR (d) parametric reconstruction (new method)

## Acknowledgements

The authors would like to thank Dr. Tie-Qiang Li, Dr. Karmen Yoder and Mr. Cristian Constantinescu at Indiana University School of Medicine for their help in making the rat phantom.

## References

- [1] Y. Zhou, C.J. Endres, J.R. Brasic, S.C. Huang, and D.F. Wong, "Linear regression with spatial constraint to generate parametric images of ligand-receptor dynamic PET studies with a simplified reference tissue model," *Neuroimage*, vol. 18, pp. 975–989, 2003.
- [2] E. D. Morris, C. J. Endres, K. C. Schmidt, B. T. Christian, R. F. Muzic Jr., and R. E. Fisher, "Kinetic modeling in PET," in *Emission Tomography:*

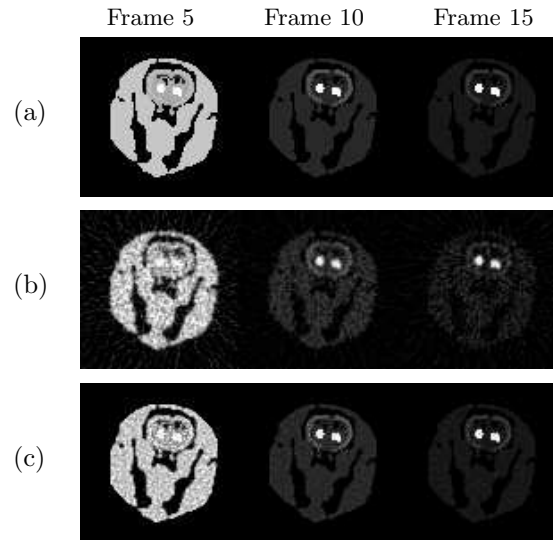


Figure 8: Emission images (a) original phantom (b) FBP reconstruction (c) parametric reconstruction (new method)

*The Fundamentals of PET and SPECT*, M. Werner and J. Aarsvold, Eds. Academic Press, San Diego, 2003.

- [3] C. A. Bouman and K. Sauer, "A unified approach to statistical tomography using coordinate descent optimization," *IEEE Trans. on Image Processing*, vol. 5, no. 3, pp. 480–492, March 1996.
- [4] G. Paxinos and C. Watson, *The Rat Brain in Stereotaxic Coordinates*, Academic Press, 4th edition, 1998.
- [5] S. Pappata, S. Dehaene, J. B. Poline, M. C. Gregoire, A. Jobert, J. Delforge, V. Frouin, M. Bottlaender, F. Dolle, L. Di Giamberardino, and A. Syrota, "In vivo detection of striatal dopamine release during reward: a PET study with [ $^{11}\text{C}$ ]raclopride and a single dynamic scan approach," *Neuroimage*, vol. 16, no. 4, pp. 1015–27, 2002.
- [6] Koon-Pong Wong, Dagan Feng, Steven R. Meikle, and Michael J. Fulham, "Simultaneous estimation of physiological parameters and the input function - in vivo PET data," *IEEE Transactions on Information Technology in Biomedicine*, vol. 5, no. 1, pp. 67–76, March 2001.